



Measurement of decay-time dependent CP violation in $B^0 \rightarrow K_S^0 K_S^0 K_S^0$ using 2019–2021 Belle II data

The Belle II Collaboration

F. Abudinén, I. Adachi, K. Adamczyk, L. Aggarwal, P. Ahlburg, H. Ahmed, J. K. Ahn, H. Aihara, N. Akopov, A. Aloisio, F. Ameli, L. Andricek, N. Anh Ky, D. M. Asner, H. Atmacan, V. Aulchenko, T. Aushev, V. Aushev, T. Aziz, V. Babu, S. Bacher, H. Bae, S. Baehr, S. Bahinipati, A. M. Bakich, P. Bambade, Sw. Banerjee, S. Bansal, M. Barrett, G. Batignani, J. Baudot, M. Bauer, A. Baur, A. Beaubien, A. Beaulieu, J. Becker, P. K. Behera, J. V. Bennett, E. Bernieri, F. U. Bernlochner, V. Bertacchi, M. Bertemes, E. Bertholet, M. Bessner, S. Bettarini, V. Bhardwaj, B. Bhuyan, F. Bianchi, T. Bilka, S. Bilokin, D. Biswas, A. Bobrov, D. Bodrov, A. Bolz, A. Bondar, G. Bonvicini, A. Bozek, M. Bračko, P. Branchini, N. Braun, R. A. Briere, T. E. Browder, D. N. Brown, A. Budano, L. Burmistrov, S. Bussino, M. Campajola, L. Cao, G. Casarosa, C. Cecchi, D. Červenkov, M.-C. Chang, P. Chang, R. Cheaib, P. Cheema, V. Chekelian, C. Chen, Y. Q. Chen, Y. Q. Chen, Y.-T. Chen, B. G. Cheon, K. Chilikin, K. Chirapatpimol, H.-E. Cho, K. Cho, S.-J. Cho, S.-K. Choi, S. Choudhury, D. Cinabro, L. Corona, L. M. Cremaldi, S. Cunliffe, T. Czank, S. Das, N. Dash, F. Dattola, E. De La Cruz-Burelo, S. A. De La Motte, G. de Marino, G. De Nardo, M. De Nuccio, G. De Pietro, R. de Sangro, B. Deschamps, M. Destefanis, S. Dey, A. De Yta-Hernandez, R. Dhamija, A. Di Canto, F. Di Capua, S. Di Carlo, J. Dingfelder, Z. Doležal, I. Domínguez Jiménez, T. V. Dong, M. Dorigo, K. Dort, D. Dossett, S. Dreyer, S. Dubey, S. Duell, G. Dujany, P. Ecker, S. Eidelman, M. Eliachevitch, D. Epifanov, P. Feichtinger, T. Ferber, D. Ferlewicz, T. Fillinger, C. Finck, G. Finocchiaro, P. Fischer, K. Flood, A. Fodor, F. Forti, A. Frey, M. Friedl, B. G. Fulsom, M. Gabriel, A. Gabrielli, N. Gabyshev, E. Ganiev, M. Garcia-Hernandez, R. Garg, A. Garmash, V. Gaur, A. Gaz, U. Gebauer, A. Gellrich, J. Gemmler, T. Geßler, G. Ghevondyan, G. Giakoustidis, R. Giordano, A. Giri, A. Glazov, B. Gobbo, R. Godang, P. Goldenzweig, B. Golob, P. Gomis, G. Gong, P. Grace, W. Gradl, S. Granderath, E. Graziani, D. Greenwald, T. Gu, Y. Guan, K. Gudkova, J. Guilleams, C. Hadjivasiliou, S. Halder, K. Hara, T. Hara, O. Hartbrich, K. Hayasaka, H. Hayashii, S. Hazra, C. Heartly, M. T. Hedges, I. Heredia de la Cruz, M. Hernández Villanueva, A. Hershenhorn, T. Higuchi, E. C. Hill, H. Hirata, M. Hoek, M. Hohmann, S. Hollitt, T. Hotta, C.-L. Hsu, K. Huang, T. Humair, T. Iijima, K. Inami, G. Inguglia, N. Ipsita, J. Irakkathil Jabbar, A. Ishikawa, S. Ito, R. Itoh, M. Iwasaki, Y. Iwasaki, S. Iwata, P. Jackson, W. W. Jacobs, D. E. Jaffe, E.-J. Jang, M. Jeandron, H. B. Jeon, Q. P. Ji, S. Jia, Y. Jin, C. Joo, K. K. Joo, H. Junkerkalefeld, I. Kadenko, J. Kahn, H. Kakuno, M. Kaleta, A. B. Kaliyar, J. Kandra, K. H. Kang, S. Kang, P. Kapusta, R.

Karl, G. Karyan, Y. Kato, H. Kawai, T. Kawasaki, C. Ketter, H. Kichimi, C. Kiesling, C.-H. Kim, D. Y. Kim, H. J. Kim, K.-H. Kim, K. Kim, S.-H. Kim, Y.-K. Kim, Y. Kim, T. D. Kimmel, H. Kindo, K. Kinoshita, C. Kleinwort, B. Knysh, P. Kodyš, T. Koga, S. Kohani, K. Kojima, I. Komarov, T. Konno, A. Korobov, S. Korpar, N. Kovalchuk, E. Kovalenko, R. Kowalewski, T. M. G. Kraetzschmar, F. Krinner, P. Križan, R. Kroeger, J. F. Krohn, P. Krokovny, H. Krüger, W. Kuehn, T. Kuhr, J. Kumar, M. Kumar, R. Kumar, K. Kumara, T. Kumita, T. Kunigo, M. Künzel, S. Kurz, A. Kuzmin, P. Kvasnička, Y.-J. Kwon, S. Lacaprara, Y.-T. Lai, C. La Licata, K. Lalwani, T. Lam, L. Lanceri, J. S. Lange, M. Laurenza, K. Lautenbach, P. J. Laycock, R. Lebourier, F. R. Le Diberder, I.-S. Lee, S. C. Lee, P. Leitl, D. Levit, P. M. Lewis, C. Li, L. K. Li, S. X. Li, Y. B. Li, J. Libby, K. Lieret, J. Lin, Z. Liptak, Q. Y. Liu, Z. A. Liu, D. Liventsev, S. Longo, A. Loos, A. Lozar, P. Lu, T. Lueck, F. Luetzicke, T. Luo, C. Lyu, C. MacQueen, M. Maggiora, R. Maiti, S. Maity, R. Manfredi, E. Manoni, A. Manthei, S. Marcello, C. Marinas, L. Martel, A. Martini, L. Massacesi, M. Masuda, T. Matsuda, K. Matsuoka, D. Matvienko, J. A. McKenna, J. McNeil, F. Meggendorfer, F. Meier, M. Merola, F. Metzner, M. Milesi, C. Miller, K. Miyabayashi, H. Miyake, H. Miyata, R. Mizuk, K. Azmi, G. B. Mohanty, N. Molina-Gonzalez, S. Moneta, H. Moon, T. Moon, J. A. Mora Grimaldo, T. Morii, H.-G. Moser, M. Mrvar, F. J. Müller, Th. Müller, G. Muroyama, C. Murphy, R. Mussa, I. Nakamura, K. R. Nakamura, E. Nakano, M. Nakao, H. Nakayama, H. Nakazawa, A. Narimani Charan, M. Naruki, Z. Natkaniec, A. Natochii, L. Nayak, M. Nayak, G. Nazaryan, D. Neverov, C. Niebuhr, M. Niiyama, J. Ninkovic, N. K. Nisar, S. Nishida, K. Nishimura, M. H. A. Nouxman, K. Ogawa, S. Ogawa, S. L. Olsen, Y. Onishchuk, H. Ono, Y. Onuki, P. Oskin, F. Otani, E. R. Oxford, H. Ozaki, P. Pakhlov, G. Pakhlova, A. Paladino, T. Pang, A. Panta, E. Paoloni, S. Pardi, K. Parham, H. Park, S.-H. Park, B. Paschen, A. Passeri, A. Pathak, S. Patra, S. Paul, T. K. Pedlar, I. Peruzzi, R. Peschke, R. Pestotnik, F. Pham, M. Piccolo, L. E. Piilonen, G. Pinna Angioni, P. L. M. Podesta-Lerma, T. Podobnik, S. Pokharel, L. Polat, V. Popov, C. Praz, S. Prell, E. Prencipe, M. T. Prim, M. V. Purohit, H. Purwar, N. Rad, P. Rados, S. Raiz, A. Ramirez Morales, R. Rasheed, N. Rauls, M. Reif, S. Reiter, M. Remnev, I. Ripp-Baudot, M. Ritter, M. Ritzert, G. Rizzo, L. B. Rizzuto, S. H. Robertson, D. Rodríguez Pérez, J. M. Roney, C. Rosenfeld, A. Rostomyan, N. Rout, M. Rozanska, G. Russo, D. Sahoo, Y. Sakai, D. A. Sanders, S. Sandilya, A. Sangal, L. Santelj, P. Sartori, Y. Sato, V. Savinov, B. Scavino, M. Schnepf, M. Schram, H. Schreeck, J. Schueler, C. Schwanda, A. J. Schwartz, B. Schwenker, M. Schwickardi, Y. Seino, A. Selce, K. Senyo, I. S. Seong, J. Serrano, M. E. Sevier, C. Sfienti, V. Shebalin, C. P. Shen, H. Shibuya, T. Shillington, T. Shimasaki, J.-G. Shiu, B. Shwartz, A. Sibidanov, F. Simon, J. B. Singh, S. Skambraks, J. Skorupa, K. Smith, R. J. Sobie, A. Soffer, A. Sokolov, Y. Soloviev, E. Solovieva, S. Spataro, B. Spruck, M. Starič, S. Stefkova, Z. S. Stottler, R. Stroili, J. Strube, J. Stypula, Y. Sue, R. Sugiura, M. Sumihama, K. Sumisawa, T. Sumiyoshi, W. Sutcliffe, S. Y. Suzuki, H. Svidras, M. Tabata, M. Takahashi, M. Takizawa, U. Tamponi, S. Tanaka, K. Tanida, H. Tanigawa, N. Taniguchi, Y. Tao, P. Taras, F. Tenchini, R. Tiwary, D. Tonelli, E. Torassa, N. Toutounji, K. Trabelsi, I. Tsaklidis, T. Tsuboyama, N. Tsuzuki, M. Uchida, I. Ueda, S. Uehara, Y. Uematsu, T. Ueno, T. Uglov, K. Unger, Y. Unno, K. Uno, S. Uno, P. Urquijo, Y. Ushiroda, Y. V. Usov, S. E. Vahsen, R. van Tonder, G. S. Varner, K. E. Varvell, A. Vinokurova, L. Vitale, V. Vobbiliseti, V.

Vorobyev, A. Vossen, B. Wach, E. Waheed, H. M. Wakeling, K. Wan, W. Wan Abdullah, B. Wang, C. H. Wang, E. Wang, M.-Z. Wang, X. L. Wang, A. Warburton, M. Watanabe, S. Watanuki, J. Webb, S. Wehle, M. Welsch, C. Wessel, J. Wiechczynski, P. Wieduwilt, H. Windel, E. Won, L. J. Wu, X. P. Xu, B. D. Yabsley, S. Yamada, W. Yan, S. B. Yang, H. Ye, J. Yelton, J. H. Yin, M. Yonenaga, Y. M. Yook, K. Yoshihara, T. Yoshinobu, C. Z. Yuan, Y. Yusa, L. Zani, Y. Zhai, J. Z. Zhang, Y. Zhang, Y. Zhang, Z. Zhang, V. Zhilich, J. Zhou, Q. D. Zhou, X. Y. Zhou, V. I. Zhukova, V. Zhulanov, and R. Žlebčík

Abstract

We report a measurement of decay-time dependent CP -violating parameters in $B^0 \rightarrow K_s^0 K_s^0 K_s^0$ decays. We use $(198.0 \pm 3.0) \times 10^6$ $B\bar{B}$ pairs collected at the $\Upsilon(4S)$ resonance with the Belle II detector at the SuperKEKB asymmetric-energy e^+e^- collider. The observed mixing-induced and direct CP violation parameters are $\mathcal{S} = -1.86^{+0.91}_{-0.46}$ (stat) ± 0.09 (syst) and $\mathcal{A} = -0.22^{+0.30}_{-0.27}$ (stat) ± 0.04 (syst), respectively.

1 Introduction

In the Standard Model (SM), the charmless three-body decay $B^0 \rightarrow K_s^0 K_s^0 K_s^0$ is mediated by the $b \rightarrow sq\bar{q}$ quark transition corresponding to a “penguin” one-loop amplitude represented by the diagram in Fig. 1 (charge-conjugate decays are implied hereafter unless specified otherwise). The three- K_s^0 final state is CP even. The small branching fraction $(6.0 \pm 0.5) \times 10^{-6}$ [1] suppressed by the penguin loop makes this decay sensitive to a possible contribution from non-SM physics [2].

Decay-time dependent CP violation arises from interference between decay amplitudes with and without mixing, due to an irreducible phase in the Cabibbo-Kobayashi-Maskawa (CKM) quark-mixing matrix [3]. If one of the neutral B mesons produced from the $\Upsilon(4S)$ decays into a CP eigenstate, f_{CP} , at time t_{CP} , and the other B meson turns into a flavor-distinguishable final state, f_{tag} , at time t_{tag} , the time-dependent decay rate is given by [4–6]

$$\mathcal{P}(\Delta t) = \frac{e^{-|\Delta t|/\tau_{B^0}}}{4\tau_{B^0}} (1 + q[\mathcal{S} \sin(\Delta m_d \Delta t) + \mathcal{A} \cos(\Delta m_d \Delta t)]), \quad (1)$$

where $\Delta t \equiv t_{CP} - t_{\text{tag}}$, and the CP -violating parameters \mathcal{S} and \mathcal{A} are related to mixing-induced and direct CP violation, respectively. We refer to the B meson decaying into f_{CP} as B_{CP} and to the other B meson as B_{tag} . The flavor q is +1 (−1) for B_{tag}^0 ($\overline{B}_{\text{tag}}^0$), τ_{B^0} is the B^0 lifetime, and Δm_d is the mass difference between the two mass eigenstates of the B^0 - \overline{B}^0 system. The SM predicts that $\mathcal{S} \approx -\sin 2\phi_1$ and $\mathcal{A} = 0$ in $B^0 \rightarrow K_s^0 K_s^0 K_s^0$, where ϕ_1 is defined in terms of the CKM matrix elements as $\phi_1 \equiv \arg[-V_{cd}V_{cb}^*/V_{td}V_{tb}^*]$. The deviation of \mathcal{S} from $-\sin 2\phi_1$ is predicted to be 0.02 with an uncertainty smaller than 0.01 [7]. The Belle [8] and BaBar [9] experiments measured these asymmetries with comparable uncertainties (25% on \mathcal{S} and 20% on \mathcal{A}), where the uncertainties are dominated by the size of their $B^0 \rightarrow K_s^0 K_s^0 K_s^0$ samples. The world average values are $\mathcal{S} = -0.83 \pm 0.17$ and $\mathcal{A} = 0.15 \pm 0.12$ [10]. The search for non-SM physics with a new CP -violating phase requires additional independent measurements with improved sensitivity.

We report a measurement of \mathcal{S} and \mathcal{A} in $B^0 \rightarrow K_s^0 K_s^0 K_s^0$ decays using a sample of $(198.0 \pm 3.0) \times 10^6$ $B\overline{B}$ pairs collected by the Belle II experiment. We reconstruct $B^0 \rightarrow K_s^0 K_s^0 K_s^0$ decays with $K_s^0 \rightarrow \pi^+\pi^-$ as B_{CP} and suppress background using two boosted decision-tree (BDT) classifiers. We then measure q using the remaining charged particles in the event and Δt from the difference between the decay positions of B_{CP} and B_{tag} . Finally, likelihood fits are performed to determine the signal yield and CP -violating parameters, respectively. We use $B^+ \rightarrow K_s^0 K_s^0 K^+$ decays as a control channel to determine fit models and to validate the fit procedure.

2 The Belle II detector and data sample

The Belle II experiment operates at the SuperKEKB asymmetric-energy e^+e^- collider [11], at KEK in Tsukuba, Japan. The Belle II detector [12] is designed to reconstruct the final-state particles from e^+e^- collisions. Detector subsystems are arranged cylindrically around the beam interaction point. The innermost subsystem is the vertex detector (VXD), which

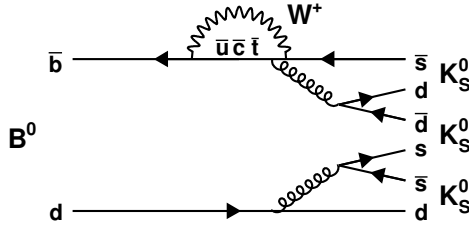


Figure 1: Leading decay amplitude for the $B^0 \rightarrow K_S^0 K_S^0 K_S^0$ decays.

consists of two inner layers of silicon pixel detectors (PXD) and four outer layers of double-sided silicon strip detectors. The second layer of the PXD is currently partially installed and covers one sixth of the design acceptance. Compared to Belle, the larger volume of the VXD is expected to provide more acceptance for K_S^0 vertexing. The main tracking device is the central drift chamber, located outside of the vertex detector. Outside of the drift chamber, two types of Cherenkov ring-imaging detectors provide hadron identification. The central volume is covered by a time-of-propagation detector, which uses quartz bars as Cherenkov radiator, and the forward endcap is covered by an aerogel radiator detector. Outside of this is the electromagnetic calorimeter, which is made up of CsI(Tl) crystals. A 1.5 T axial magnetic field is generated by a superconducting solenoid surrounding the calorimeter. The outermost subsystem is the K_L^0 and muon detector, which consists of iron plates interspersed with resistive plate chambers and scintillators. Muons and K_L^0 's are detected through their interactions with the material. The iron plates also serve as the return yoke for the magnetic field.

We use a data set collected at the $\Upsilon(4S)$ resonance in 2019–2021. The data set corresponds to an integrated luminosity of 189.3 fb^{-1} and contains $(198.0 \pm 3.0) \times 10^6 B\bar{B}$ pairs. We use two types of Monte Carlo (MC) simulation samples to optimize selection criteria and to train BDTs used for event reconstruction. In one sample $B^0\bar{B}^0$ pairs are generated, with one of the B mesons decaying to the signal mode. The signal MC sample is also used to determine models for the likelihood fit to the Δt and q distributions. The other sample includes $e^+e^- \rightarrow q\bar{q}$ ($q = u, d, s, c$), $B^0\bar{B}^0$, and B^+B^- events that proceed with realistic hadronization and decay processes. We use the EvtGen [13] package to simulate hadron decays and KKMC [14] with Pythia [15] for $q\bar{q}$. The detector response is simulated by Geant4 [16]. Both data and MC samples are analyzed with the Belle II analysis software framework [17].

3 Event reconstruction

The $\Upsilon(4S)$ is produced at the collision point with a Lorentz boost ($\beta\gamma$) of 0.287, and subsequently decays to B and \bar{B} mesons, which are nearly at rest in the center-of-mass (CM) frame. Therefore, the B meson pairs propagate in the laboratory nearly along the boost direction with a known boost factor, which enables us to approximate the decay-time difference between them as $\Delta t = (\ell_{CP} - \ell_{\text{tag}})/\beta\gamma$. Here, $\ell_{CP(\text{tag})}$ is the decay position of $B_{CP(\text{tag})}$ which is projected onto the boost axis.

Pairs of oppositely charged particles with dipion mass between $457.6 \text{ MeV}/c^2$ and

537.6 MeV/c² are used to reconstruct $K_s^0 \rightarrow \pi^+\pi^-$ candidates. The K_s^0 properties are obtained from a kinematic fit of the π^+ and π^- trajectories. To reduce the combinatorial background from incorrectly reconstructed (“fake”) K_s^0 candidates, a discriminant variable is formed from a BDT classifier with 22 input variables that include kinematic quantities, particle identification information, and the number of hits in the VXD associated to the π^\pm tracks, which are referred to as VXD hits. The most discriminating variables are the angle between the directions of K_s^0 momentum and the decay position seen from the IP in the laboratory frame, and the flight length of K_s^0 normalized by its uncertainty. A selection based on this BDT discriminant accepts 95% of correctly reconstructed (“true”) K_s^0 mesons and 0.59% of fake K_s^0 mesons. Using a fit to the dipion-mass distribution in data, we confirm that the signal efficiency is consistent with MC. Although the selection slightly biases τ_{B^0} , it does not significantly affect \mathcal{S} and \mathcal{A} . We take this effect into account as a source of systematic uncertainty.

We reconstruct B candidates by combining three K_s^0 candidates. We select B candidates using the invariant mass $M(K_s^0 K_s^0 K_s^0)$ and beam-energy-constrained mass $M_{bc} \equiv \sqrt{E_{\text{beam}}^2 - |\vec{p}_B|^2}$, where E_{beam} and \vec{p}_B are the beam energy and the momentum of B meson in the CM frame. The difference between the beam energy ($\sqrt{s}/2$) and the reconstructed B energy in the CM frame, $\Delta E \equiv E_{\text{beam}} - E_B$, is not used because of its correlation with M_{bc} . We retain the B candidates satisfying $5.2 < M_{bc} < 5.29 \text{ GeV}/c^2$ and $5.08 < M(K_s^0 K_s^0 K_s^0) < 5.48 \text{ GeV}/c^2$, but exclude the candidates satisfying $5.265 < M_{bc} < 5.29 \text{ GeV}/c^2$ and $5.08 < M(K_s^0 K_s^0 K_s^0) < 5.181 \text{ GeV}/c^2$ to avoid contamination by background due to $B^{0(+)} \rightarrow K_s^0 K_s^0 K^{*0(+)}$.

The dominant source of background arises from continuum $e^+e^- \rightarrow q\bar{q}$ events. We suppress the continuum background using another BDT classifier \mathcal{O}'_{CS} with the following input variables related to event topology: the cosine of the angle between the thrust axes of B_{CP} and B_{tag} ; the magnitude of the thrust of B_{tag} ; the sum of the transverse momenta of the particles in the event; missing mass squared; and modified Fox-Wolfram moments [18]. Here, the thrust axis of a B meson is a unit vector \vec{t} that maximizes the thrust magnitude $T \equiv (\sum_i |\vec{t} \cdot \vec{p}_i|) / (\sum_i |\vec{p}_i|)$, where \vec{p}_i is the momentum of the B meson i th daughter. The selection on \mathcal{O}'_{CS} rejects 49% of background and retains 98% of signal. The selection criteria for K_s^0 candidates are determined by maximizing a figure of merit, $N_{\text{sig}} / \sqrt{N_{\text{sig}} + N_{\text{bkg}}}$, where N_{sig} and N_{bkg} are the yields of simulated signal and background events, respectively, satisfying $5.27 < M_{bc} < 5.29 \text{ GeV}/c^2$, $5.18 < M(K_s^0 K_s^0 K_s^0) < 5.38 \text{ GeV}/c^2$, and $\mathcal{O}'_{CS} > 0.5$.

In addition to the non-resonant decay amplitude, quasi-two-body decays $B^0 \rightarrow X(\rightarrow K_s^0 K_s^0)K_s^0$ due to $b \rightarrow s$ and $b \rightarrow c$ transitions contribute to $B^0 \rightarrow K_s^0 K_s^0 K_s^0$ decays. Since we regard the decays via $b \rightarrow s$ as signal, we veto the $b \rightarrow c$ contribution to measure the CP violation in a pure $b \rightarrow s$ process. We only expect a significant $b \rightarrow c$ contribution from $\chi_{c0} K_s^0$. The branching ratio of $B^0 \rightarrow \chi_{c0}(\rightarrow K_s^0 K_s^0)K_s^0$ is around 5% of the signal branching ratio. We reject B^0 candidates if the invariant mass of any combination of two K_s^0 candidates is in the range $3379 < M(K_s^0 K_s^0) < 3447 \text{ MeV}/c^2$. This requirement rejects 90% of the background from $B^0 \rightarrow \chi_{c0} K_s^0$ and 7.5% of signal.

4 Measurement of B -meson flavor and decay-time difference

We use a BDT-based algorithm to identify the B_{tag} flavor [19]. It uses 13 BDTs, each of which extracts a specific signature of $b \rightarrow c \rightarrow s$ cascade decays from the particle identification and kinematic variables of particles not belonging to B_{CP} . The outputs from the BDTs are combined by a higher-level BDT to return the value of q (defined earlier) and a tagging quality variable r . The variable r varies from zero for no tagging information to one for unambiguous flavor assignment. The probability density function (PDF) for signal events is represented as a modified version of Eq. (1) by the probability to misidentify the flavor, w , and its difference between B^0 and \bar{B}^0 , Δw ,

$$\mathcal{P}_{\text{sig}}^{\text{TD}}(\Delta t, q) = \frac{e^{-|\Delta t|/\tau_{B^0}}}{4\tau_{B^0}} \left(1 - q\Delta w + (1 - 2w)q[\mathcal{S} \sin(\Delta m_d \Delta t) + \mathcal{A} \cos(\Delta m_d \Delta t)] \right). \quad (2)$$

The events are classified into seven independent r intervals. For each of these intervals, w and Δw are determined using flavor-specific B -meson decays with large branching fractions [19].

To measure Δt , we reconstruct the decay vertices of B_{CP} and B_{tag} using information about the beam interaction point (IP), which is modeled by a three-dimensional Gaussian distribution. The B_{CP} vertex position is reconstructed from K_s^0 daughter tracks and the reconstructed B_{CP} trajectory that originates from the IP and points toward the reconstructed B_{CP} momentum. Often K_s^0 mesons decay outside of the VXD volume resulting in less well-measured decay positions. Hence, the B_{CP} vertex resolution largely depends on the number of K_s^0 mesons that have associated VXD hits. In the signal MC, the fractions of events where zero, one, two, and three K_s^0 candidates have VXD hits are 0.4%, 8.0%, 37.7%, and 54.0%, respectively. When only one K_s^0 has VXD hits, the B_{CP} trajectory helps to significantly improve the B_{CP} vertex resolution, reducing the average vertex position uncertainty from around 270 μm to 130 μm .

We use the tracks that do not belong to B_{CP} to reconstruct the B_{tag} vertex, excluding the tracks without an associated PXD hit and those that, combined in opposite charge pairs, yield the K_s^0 mass. Similarly to the B_{CP} vertexing, we reconstruct the B_{tag} trajectory using the IP information and B_{tag} momentum, which is calculated as the difference between the beam momentum and the B_{CP} momentum [20]. The B_{tag} trajectory is included in the vertex fit to improve the vertex resolution and reconstruction efficiency. We use the χ^2 per degree of freedom of the vertex fit χ^2/N and the vertex position uncertainty σ_ℓ as indicators of the quality of the Δt measurement. The number N_{tracks} of tracks in the fit, typically six, determines N as $N = 2N_{\text{tracks}} - 1$. We require $\chi^2/N < 100$ and $\sigma_\ell < 500 \mu\text{m}$ for B_{tag} .

The multiplicity of B_{CP} candidates in a selected event is 1.06 on average. For events with multiple candidates, we choose the one with the smallest B_{CP} vertex fit χ^2 , which is not correlated with the true Δt .

We apply the following selection criteria, related to the B_{CP} vertex and Δt , to the remaining candidates: one or more K_s^0 from B_{CP} is associated with VXD hits; if a K_s^0 daughter track from B_{CP} is associated with a hit in the first PXD layer (layer-1 hit), its partner from the same K_s^0 should also have a layer-1 hit; otherwise it is likely the

layer-1 hit belongs to a particle that was incorrectly associated to B_{CP} , degrading the B_{CP} vertex resolution; the χ^2 probability of the vertex fit should be larger than 0.001 for B_{CP} ; $\sigma_\ell < 500 \mu\text{m}$ for B_{CP} ; and $-30 < \Delta t < 30$ ps. We call the events passing these criteria time-differential (TD) events and the others time-integrated (TI) events. We use the B_{tag} flavor information for TI events, but not the Δt information. Therefore, the PDF in Eq. (2) is integrated over Δt for TI events,

$$\mathcal{P}_{\text{sig}}^{\text{TI}}(q) = \frac{1}{2} \left(1 - q\Delta w + (1 - 2w)q\mathcal{A} \frac{1}{1 + \Delta m_d^2 \tau_{B^0}^2} \right). \quad (3)$$

5 Determination of signal yield

We extract the signal yields for TD and TI events separately from three-dimensional likelihood fits to the unbinned distributions of M_{bc} , $M(K_s^0 K_s^0 K_s^0)$, and \mathcal{O}'_{CS} . The likelihood function accounts for two sample components, signal and background. For the signal component, the M_{bc} distribution is modeled with a Gaussian function, the $M(K_s^0 K_s^0 K_s^0)$ distribution with the sum of two Gaussian functions, and the \mathcal{O}'_{CS} distribution with an asymmetric Gaussian function. We determine the parameters for the signal shapes with fits to the signal MC sample. We use different parameter sets for the $M(K_s^0 K_s^0 K_s^0)$ distribution in TD and TI events because the latter have a broader distribution due to poorly reconstructed candidates. For the background component, the M_{bc} distribution is modeled with an ARGUS function [21], the $M(K_s^0 K_s^0 K_s^0)$ distribution with a linear function, and the \mathcal{O}'_{CS} distribution with the sum of a Gaussian function and an asymmetric Gaussian function.

We use $B^+ \rightarrow K_s^0 K_s^0 K^+$ decays to determine the background parameters because their kinematic properties are similar to those of the signal decay. The background PDF shapes are confirmed to be consistent between the two decay modes using MC samples. The fit for $B^+ \rightarrow K_s^0 K_s^0 K^+$ gives both the corresponding yield, used as a validation of our fitting procedures, and the background PDF parameters for the $B^0 \rightarrow K_s^0 K_s^0 K_s^0$ fit.

Figure 2 shows the results of fits to $B^0 \rightarrow K_s^0 K_s^0 K_s^0$ decays, separated into TD and TI samples. We define the signal region as $5.271 < M_{\text{bc}} < 5.288 \text{ GeV}/c^2$, $5.181 < M(K_s^0 K_s^0 K_s^0) < 5.366 \text{ GeV}/c^2$, and $-3.945 < \mathcal{O}'_{CS} < 5.807$ so that each range retains 99.73% of signal TD events. The signal yield is 53 ± 8 events and the purity is 54% in the signal region for TD events, and 48_{-7}^{+8} events and 45% for TI events.

6 Determination of CP -violating parameters

We determine the CP -violating parameters \mathcal{S} and \mathcal{A} by an unbinned maximum-likelihood fit to the Δt and q distributions combining TD and TI events restricted to the signal region. The contribution to the likelihood function from the j th TD event is

$$\mathcal{P}_j^{\text{TD}}(\Delta t_j, q_j) = f_j^{\text{sig}} \int d(\Delta t') R(\Delta t_j - \Delta t') \mathcal{P}_{\text{sig}}(\Delta t', q_j) + (1 - f_j^{\text{sig}}) \mathcal{P}_{\text{bkg}}(\Delta t_j), \quad (4)$$

where $R(\delta\Delta t)$ is the response function of the Δt measurement, f_j^{sig} is the signal fraction of the j th event, and \mathcal{P}_{bkg} is the Δt distribution of background events. The response function

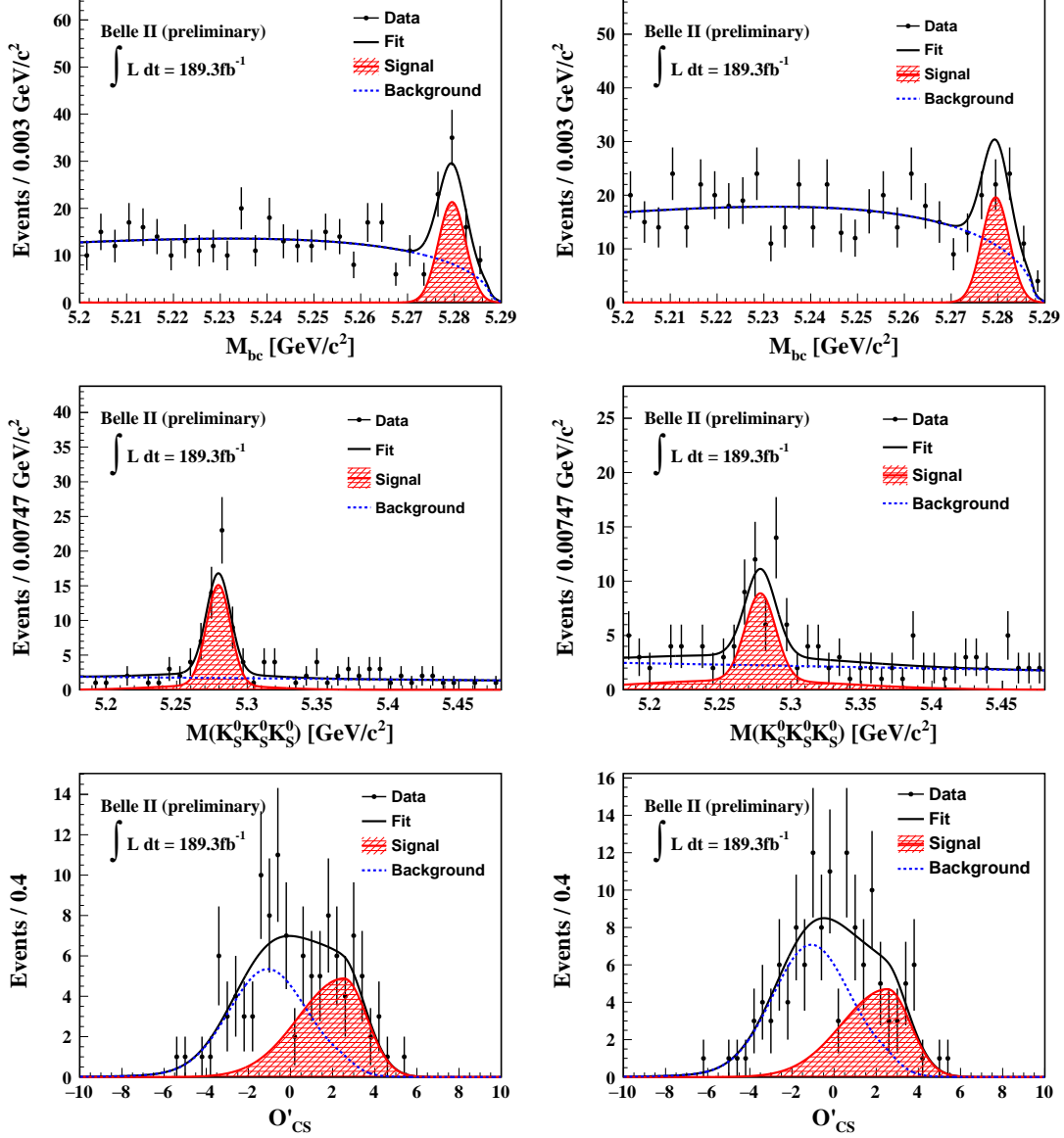


Figure 2: Distributions of (top) M_{bc} , (middle) $M(K_S^0 K_S^0 K_S^0)$, and (bottom) O'_{CS} for (left) TD candidates and (right) TI candidates with fit projections overlaid. The M_{bc} distributions are restricted to events in the $M(K_S^0 K_S^0 K_S^0)$ signal region. The $M(K_S^0 K_S^0 K_S^0)$ and O'_{CS} distributions are restricted to events in the M_{bc} signal region.

consists of three components: detector resolutions for B_{CP} and B_{tag} , bias due to secondary tracks from charmed intermediate states for B_{tag} , and a correction to the boost factors due to their small, but non-zero, CM momentum. The parameters for the response function are fixed to the values obtained from a fit to signal MC events. We calculate f_j^{sig} from the signal-extraction fit including the tagging probability r and the cosine of the polar angle of the B_{CP} momentum in the CM frame. The additional variables are introduced to avoid fit biases due to implicitly considering equal distributions that differ across sample components [22]. The r distribution for the background component is obtained from the $M_{\text{bc}} < 5.265 \text{ GeV}/c^2$ sideband of the control channel. The distribution \mathcal{P}_{bkg} is modeled in the same way as the response function component for the detector resolution. Its parameters are determined by a fit to the data sideband, $M_{\text{bc}} < 5.265 \text{ GeV}/c^2$. For TI events, we use the likelihood function of Eq. (4) integrated over Δt ,

$$\mathcal{P}_j^{\text{TI}}(q_j) = f_j^{\text{sig}} \mathcal{P}_{\text{sig}}^{\text{TI}}(q_j) + \frac{1 - f_j^{\text{sig}}}{2}. \quad (5)$$

To validate the analysis procedure, we reconstruct $B^+ \rightarrow K_s^0 K_s^0 K^+$ decays without using the position information of K^+ in the vertex fit and extract \mathcal{S} while fixing \mathcal{A} at zero. The result $\mathcal{S} = 0.37_{-0.33}^{+0.31}$ is consistent with no CP violation and thus supports the robustness of our analysis procedure. Only TD events are used in the fit for the control channel.

Using $B^0 \rightarrow K_s^0 K_s^0 K_s^0$ decays, we obtain $\mathcal{S} = -1.86_{-0.52}^{+0.60}$ and $\mathcal{A} = -0.22_{-0.21}^{+0.22}$, where the uncertainties are statistical. The uncertainties are known to be underestimated by the fit due to the small sample size. We reevaluate them using a parametric bootstrap method, in which we generate simplified simulated experiments obtained by sampling the likelihood, with the most probable \mathcal{S} and \mathcal{A} within the physical region $\mathcal{S}^2 + \mathcal{A}^2 \leq 1$ as input parameters. We obtain the distribution of \mathcal{S} and \mathcal{A} from the simplified simulated experiments and define the statistical uncertainty using 16 and 84 percentiles of the distribution. The estimated uncertainties are $_{-0.46}^{+0.91}$ for \mathcal{S} and $_{-0.27}^{+0.30}$ for \mathcal{A} . Figure 3 shows the signal component of the Δt distribution separated for $q = \pm 1$ using an $sPlot$ technique [23] and the asymmetry of the distribution. The asymmetry is defined as $\frac{N_+(\Delta t) - N_-(\Delta t)}{N_+(\Delta t) + N_-(\Delta t)}$, where $N_{\pm}(\Delta t)$ represent the number of entries with $q = \pm 1$ in the corresponding Δt bin. The plots show only TD events.

7 Systematic uncertainties

We consider various sources of systematic uncertainties and summarize them in Table 1. To evaluate the systematic uncertainty on \mathcal{S} and \mathcal{A} related to assumptions made on parameters of the fit model, we repeat the fit on data using alternative values of the parameters randomly sampled based on auxiliary knowledge. This approach is used for w and Δw (referred to as flavor tagging in the table), the parameters describing the resolution function, τ_{B^0} and Δm_d (physics parameters), the parameters for the M_{bc} , $M(K_s^0 K_s^0 K_s^0)$, and \mathcal{O}'_{CS} shapes (signal fraction), and the parameters for the background Δt shape. The widths of the resulting distributions of \mathcal{S} and \mathcal{A} are taken as contributions to the systematic uncertainty. We use the world-average values and uncertainties of τ_{B^0} and Δm_d [1]

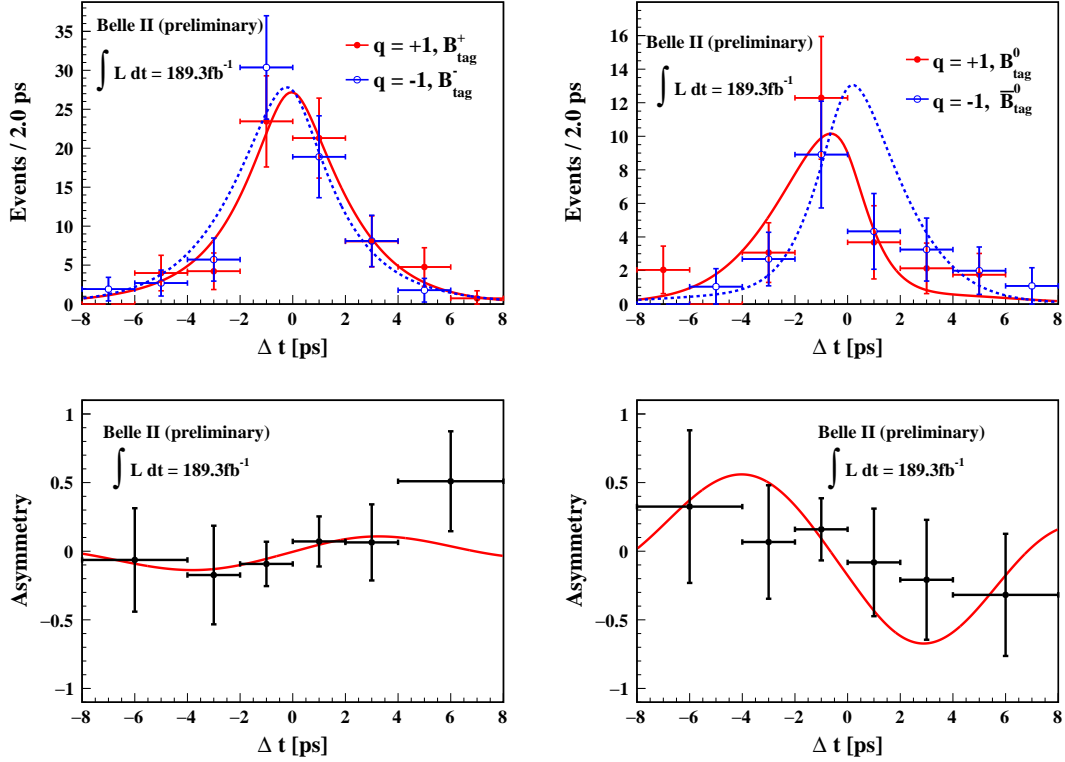


Figure 3: (top) Δt distribution of the signal component extracted with the $sPlot$ technique and (bottom) its asymmetry for (left) $B^+ \rightarrow K_s^0 K_s^0 K^+$ candidates and (right) $B^0 \rightarrow K_s^0 K_s^0 K_s^0$ candidates. Only TD events are shown. In the Δt distribution graphs, the red solid curve and filled circles represent the fit result and data for $q = +1$, while the blue dashed curve and open circles represent the fit result and data for $q = -1$, respectively. The asymmetry is defined as $\frac{N_+(\Delta t) - N_-(\Delta t)}{N_+(\Delta t) + N_-(\Delta t)}$, where $N_{\pm}(\Delta t)$ represent the number of entries with $q = \pm 1$ in the corresponding Δt bin. In the asymmetry graphs, the points represent data and the solid curve represents the result of the fit.

and modify the τ_{B^0} uncertainty considering the bias due to the K_s^0 selection.

The systematic uncertainty due to the vertex reconstruction is determined by varying the parameters for the IP profile and boost vector, track requirements for the B_{tag} vertex reconstruction, criteria to select TD events, and correction of helix parameter uncertainties for vertexing. We use MC samples simulated with a misaligned detector geometry to evaluate the misalignment effect. The systematic uncertainty on the resolution model is determined by analyzing a MC sample with alternative models of Δt response functions. Correlations are observed between $M(K_s^0 K_s^0 K_s^0)$ and χ^2/N for B_{CP} , and between \mathcal{O}'_{CS} and flavor tag. For the systematic uncertainty due to the fit bias, two sets of simplified simulated experiments are generated with and without these correlations; the fits for \mathcal{S} and \mathcal{A} are performed ignoring these correlations. We take the difference between the mean value of \mathcal{S} and \mathcal{A} for the two sets as a systematic uncertainty. For tag-side interference [24], simplified simulated experiments are generated with and without tag-side interference and the difference is taken as a systematic uncertainty. The systematic

Table 1: Systematic uncertainties

Source	$\delta\mathcal{S}$	$\delta\mathcal{A}$
Vertex reconstruction	0.025	0.022
Flavor tagging	0.079	0.030
Resolution function	0.012	0.006
Physics parameters	0.008	0.000
Fit bias	0.003	0.002
Signal fraction	0.011	0.007
Background Δt shape	0.011	0.001
Detector misalignment	0.002	0.004
Resolution model	0.001	0.003
Tag-side interference	0.014	0.015
Total	0.087	0.042

uncertainty is dominated by that of the flavor tagging performance owing to the limited size of the calibration sample.

8 Conclusion

In summary, we report a measurement of decay-time dependent CP violation in $B^0 \rightarrow K_s^0 K_s^0 K_s^0$ decays using a data set corresponding to $(198.0 \pm 3.0) \times 10^6$ $B\bar{B}$ pairs collected with the Belle II experiment. The measured CP -violating parameters are

$$\mathcal{S} = -1.86_{-0.46}^{+0.91} \text{ (stat)} \pm 0.09 \text{ (syst)} \text{ and} \quad (6)$$

$$\mathcal{A} = -0.22_{-0.27}^{+0.30} \text{ (stat)} \pm 0.04 \text{ (syst)}. \quad (7)$$

Figure 4 shows the confidence regions based on likelihood-ratio ordering, where both the statistical and systematic uncertainties are taken into account [25]. Here, we constrain \mathcal{S} and \mathcal{A} within the physical boundary, $\mathcal{S}^2 + \mathcal{A}^2 \leq 1$. The filled and open black circles indicate the most probable values for \mathcal{S} and \mathcal{A} in the physical region and the SM prediction $(\mathcal{S}, \mathcal{A}) = (-\sin 2\phi_1, 0)$ based on measurements in $B^0 \rightarrow (c\bar{c})K^0$ decays, respectively [10]. The results are consistent with the latest measurements at Belle and BaBar.

Acknowledgements

We thank the SuperKEKB group for the excellent operation of the accelerator, the KEK cryogenics group for the efficient operation of the solenoid, and the KEK computer group for on-site computing support.

References

- [1] P. A. Zyla et al., (Particle Data Group), *Review of Particle Physics*, PTEP **2020** (2020) 083C01.

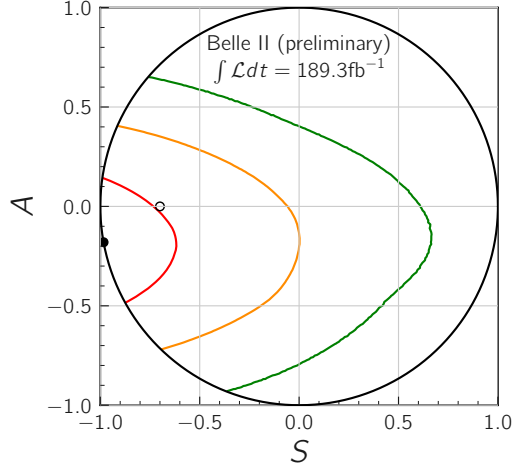


Figure 4: The red, orange, and green contours represent the 68.27%, 95.45%, and 99.73% confidence regions for \mathcal{S} and \mathcal{A} given the physical constraint $\mathcal{S}^2 + \mathcal{A}^2 \leq 1$. The filled and open black circles indicate the most probable values for \mathcal{S} and \mathcal{A} in the physical region and the SM prediction $(\mathcal{S}, \mathcal{A}) = (-\sin 2\phi_1, 0)$ based on measurements in $B^0 \rightarrow (c\bar{c})K^0$ decays, respectively [10].

- [2] Y. Grossman and M. P. Worah, *CP asymmetries in B decays with new physics in decay amplitudes*, Phys. Lett. B **395** (1997) 241, [arXiv:hep-ph/9612269](#).
- [3] M. Kobayashi and T. Maskawa, *CP Violation in the Renormalizable Theory of Weak Interaction*, Prog. Theor. Phys. **49** (1973) 652.
- [4] A. B. Carter and A. I. Sanda, *CP Violation in Cascade Decays of B Mesons*, Phys. Rev. Lett. **45** (1980) 952.
- [5] A. B. Carter and A. I. Sanda, *CP Violation in B Meson Decays*, Phys. Rev. D **23** (1981) 1567.
- [6] I. I. Y. Bigi and A. I. Sanda, *Notes on the Observability of CP Violations in B Decays*, Nucl. Phys. B **193** (1981) 85.
- [7] H. Y. Cheng, C. K. Chua, and A. Soni, *CP-violating asymmetries in B^0 decays to $K^+K^-K_{S(L)}^0$ and $K_S^0K_S^0K_{S(L)}^0$* , Phys. Rev. D **72** (2005) 094003, [arXiv:hep-ph/0506268](#).
- [8] K. H. Kang et al., (Belle collaboration), *Measurement of time-dependent CP violation parameters in $B^0 \rightarrow K_S^0K_S^0K_S^0$ decays at Belle*, Phys. Rev. D **103** (2021) 032003, [arXiv:2011.00793 \[hep-ex\]](#).
- [9] J. P. Lees et al., (BaBar collaboration), *Amplitude analysis and measurement of the time-dependent CP asymmetry of $B^0 \rightarrow K_S^0K_S^0K_S^0$ decays*, Phys. Rev. D **85** (2012) 054023, [arXiv:1111.3636 \[hep-ex\]](#).

- [10] Y. S. Amhis et al., (HFLAV), *Averages of b -hadron, c -hadron, and τ -lepton properties as of 2018*, Eur. Phys. J. **C81** (2021) 226, arXiv:1909.12524 [hep-ex]. updated results and plots available at <https://hflav.web.cern.ch/>.
- [11] K. Akai, K. Furukawa, and H. Koiso, (SuperKEKB), *SuperKEKB Collider*, Nucl. Instrum. Meth. **A907** (2018) 188, arXiv:1809.01958 [physics.acc-ph].
- [12] T. Abe et al., (Belle II Collaboration), *Belle II Technical Design Report*, arXiv:1011.0352 [physics.ins-det].
- [13] D. J. Lange, *The EvtGen particle decay simulation package*, Nucl. Instrum. Meth. **A462** (2001) 152.
- [14] S. Jadach, B. F. L. Ward, and Z. Was, *The Precision Monte Carlo event generator KK for two fermion final states in e^+e^- collisions*, Comput. Phys. Commun. **130** (2000) 260, arXiv:hep-ph/9912214 [hep-ph].
- [15] T. Sjöstrand, S. Ask, J. R. Christiansen, R. Corke, N. Desai, P. Ilten, S. Mrenna, S. Prestel, C. O. Rasmussen, and P. Z. Skands, *An Introduction to PYTHIA 8.2*, Comput. Phys. Commun. **191** (2015) 159, arXiv:1410.3012 [hep-ph].
- [16] S. Agostinelli et al., (GEANT4), *GEANT4: A Simulation toolkit*, Nucl. Instrum. Meth. **A506** (2003) 250.
- [17] T. Kuhr, C. Pulvermacher, M. Ritter, T. Hauth, and N. Braun, (Belle-II Framework Software Group), *The Belle II Core Software*, Comput. Softw. Big Sci. **3** (2019) 1, arXiv:1809.04299 [physics.comp-ph].
- [18] S. H. Lee et al., (Belle collaboration), *Evidence for $B^0 \rightarrow \pi^0\pi^0$* , Phys. Rev. Lett. **91** (2003) 261801, arXiv:hep-ex/0308040.
- [19] F. Abudinén et al., (Belle II collaboration), *B -flavor tagging at Belle II*, Eur. Phys. J. C **82** (2022) 283, arXiv:2110.00790 [hep-ex].
- [20] S. Dey and A. Soffer, *Beam-Constrained Vertexing for B Physics at the Belle II Experiment*, Springer Proc. Phys. **248** (2020) 411.
- [21] H. Albrecht et al., (ARGUS collaboration), *Search for Hadronic $b \rightarrow u$ Decays*, Phys. Lett. B **241** (1990) 278.
- [22] G. Punzi, *Comments on likelihood fits with variable resolution*, eConf **C030908** (2003) WELT002, arXiv:physics/0401045.
- [23] M. Pivk and F. R. Le Diberder, *SPlot: A Statistical tool to unfold data distributions*, Nucl. Instrum. Meth. A **555** (2005) 356, arXiv:physics/0402083.
- [24] O. Long, M. Baak, R. N. Cahn, and D. P. Kirkby, *Impact of tag side interference on time dependent CP asymmetry measurements using coherent $B^0\bar{B}^0$ pairs*, Phys. Rev. D **68** (2003) 034010, arXiv:hep-ex/0303030.

- [25] G. J. Feldman and R. D. Cousins, *A Unified approach to the classical statistical analysis of small signals*, Phys. Rev. D **57** (1998) 3873, [arXiv:physics/9711021](https://arxiv.org/abs/physics/9711021).